Available online at www.sciencedirect.com
SCIENCE DIRECT®
International Journal of Heat and Mass Transfer 48 (2005) 986–999
International Journal of HEAT and MASS TRANSFER
www.elsevier.com/locate/ijhmt

Numerical model of evaporative cooling processes in a new type of cooling tower

A.S. Kaiser [a,*], M. Lucas [b], A. Viedma [a], B. Zamora [a]

[a] Dpto. de Ingeniería Térmica y de Fluidos, Universidad Politécnica de Cartagena, Dr Fleming s/n, 30202 Cartagena, Spain
[b] Dpto. de Ingeniería de Sistemas Industriales, Universidad Miguel Hernández, Av. de la Universidad, s/n, Edificio Torreblanca, 03202 Elche, Spain

Received 2 June 2004
Available online 8 December 2004

Abstract

A numerical model for studying the evaporative cooling processes that take place in a new type of cooling tower has been developed. In contrast to conventional cooling towers, this new device called Hydrosolar Roof presents lower droplet fall and uses renewable energy instead of fans to generate the air mass flow within the tower. The numerical model developed to analyse its performance is based on computational flow dynamics for the two-phase flow of humid air and water droplets. The Eulerian approach is used for the gas flow phase and the Lagrangian approach for the water droplet flow phase, with two-way coupling between both phases. Experimental results from a full-scale prototype in real conditions have been used for validation. The main results of this study show the strong influence of the average water drop size on efficiency of the system and reveal the effect of other variables like wet bulb temperature, water mass flow to air mass flow ratio and temperature gap between water inlet temperature and wet bulb temperature. Nondimensional numerical correlation of efficiency as a function of these significant parameters has been calculated.

Keywords: Drop size; Air-conditioning; Solar chimney; Cooling tower; Solar energy

1. Introduction

Air-conditioning systems of buildings and other industrial facilities commonly use water as a heat "drain" to remove heat from refrigerant condensers. Classical solutions to reduce the temperature of this service water are usually mechanical draught-cooling towers. In general, the height of these systems ranges between 2 and 12 m. They are basically composed of shell, water distribution system, water collecting pond, fan to create the artificial draught and, in many cases, the filling.

Careful and accurate analyses of cooling towers are desirable to ensure a precise determination of their performance. The fundamentals of the physical phenomena that take place in these systems are described by Merkel [1] and subsequently by Nottage [2]. Other authors, like Mohiuddin and Kant [3] have contributed with studies about the cooling tower systematic design. Fisenko et al. [4] present a new mathematical model of a mechanical draught cooling tower performance. Benton and Waldrop [5] develop a numerical simulation of transport

* Corresponding author. Fax: +34 968 325 999.
E-mail address: antonio.kaiser@upct.es (A.S. Kaiser).

0017-9310/$ - see front matter © 2004 Elsevier Ltd. All rights reserved.
doi:10.1016/j.ijheatmasstransfer.2004.09.047

Nomenclature

A_p	droplet area (m^2)
C_D	drag coefficient
C_v	vapor concentration in bulk gas (mol/m^3)
$C_{v,s}$	vapor concentration on droplet surface (mol/m^3)
C_p	heat capacity of droplet (J/kg K)
$D_{v,m}$	diffusion coefficient of vapor in mixture (m^2/s)
D_p	droplet diameter (μm)
$\overline{D}$	average droplet diameter (μm)
e	internal energy (J/kg)
F_i	momentum source ($kg/m^2 s^2$)
$F_D(V - V_p)$	drag force per unit droplet mass (m/s^2)
g_i	gravity (m/s^2)
h	convective heat transfer coefficient ($W/m^2 K$)
h_f	latent heat of water (J/kg)
h_s	saturated air enthalpy (J/kg)
h_f	sensible enthalpy of species i' (J/kg)
H	height of droplets fall (m)
$J_{i',i}$	diffusion flux of species i' ($kg/m^2 s$)
k	thermal conductivity (W/m K)
K_c	mass transfer coefficient (m/s)
$\dot{m}_a$	air mass flow (kg/s)
$m_{i'}$	local mass fraction of species i'
m_p	mass of droplet (kg)
$\overline{m}_p$	average mass of droplet in d∀ (kg)
m_{p_0}	initial mass of droplet (kg)
$\dot{m}_{p_0}$	mass flow of droplets contained in a differential of volume d∀ (kg)
$\dot{m}_w$	water mass flow (kg/s)
Δm_p	droplet mass change in each volume differential d∀ (kg)
M_{D_p}	accumulated fraction of water droplets
M_v	molecular weight of vapor (kg/mol)
n	fit coefficient in Rosin–Rambler's equation
N_v	molar flux of vapor ($mol/m^2 s$)
Nu	Nusselt number
p	static pressure (Pa)
p_{vs}	saturated vapor pressure (Pa)
p_v	vapor pressure (Pa)
p_∞	hydrostatic pressure distribution (Pa)
P	relative static pressure (Pa)
R	universal gas constant ($kg m^2/s^2 K mol$)
r_p	droplet trajectory (m)
Re	Reynolds number
Sc	Schmidt number
$S_{i'}$	mass flow source ($kg/m^3 s$)
S_h	volumetric heat source ($kg/s^3 m$)
T	air temperature (K)
T_{in}	inlet water temperature (°C)
T_{out}	outlet water temperature (°C)
$T_{out\text{-}pr}$	predicted outlet water temperature (°C)
$T_{out\text{-}me}$	predicted outlet water temperature (°C)
T_p	temperature of the droplet (K)
T_{ref}	reference temperature for enthalpy (K)
T_{wall}	channel wall temperature (K)
T_{wb}	wet bulb temperature (°C)
T_∞	ambient temperature of continuous phase at domain inlet (K)
ΔT	temperature difference between water at inlet and outlet (°C)
ΔT_{max}	temperature difference between water inlet temperature and wet bulb temperature (°C)
ΔT_p	temperature change of droplet in d∀ (K)
ΔT_{wall}	temperature difference between channel walls and environment (°C)
u	air velocity component at the x axis (m/s)
U_{wind}	wind velocity (m/s)
v	air velocity component at the y axis (m/s)
V	air velocity (m/s)
v_i	air velocity components in the continuous phase (m/s)
V_p	droplet velocity (m/s)
x_b	x coordinate at the exit of the channel (m)
x_v	mass fraction of vapor

Greek symbols

η	efficiency
η_{me}	measured efficiency
η_{pr}	predicted efficiency
ψ	relative humidity (%)
Φ_v	Rayleigh dissipation function ($kg/s^3 m$)
μ	dynamic viscosity of air (kg/m s)
ρ	density in the continuous phase (kg/m^3)
ρ_p	density of the droplet (kg/m^3)

Subscripts

a	air
i'	species
me	measured
p	for droplet (particle)
pr	predicted
v	vapor
w	water

phenomena in evaporative cooling towers through a model that is validated with experimental data. Shesa and Mani [6] present a numerical technique for evaluating the performance of a forced convective evaporation

system. Gan and Riffat [7] develop a numerical model for determining the thermal hydraulic performance of evaporative mechanical draft cooling towers.

Other authors have centred their investigations on specific parts of these systems. Kalogirou [8] analyses the behaviour of the water sprays and shows the design of a new low-cost spray-type for a seawater evaporator. Badran [9] evaluates the influence of climate in the performance of cool towers. Milosavljevic and Heikkila [10] simulate the flow in cooling towers with CFD software, reflecting both convective and heat and mass transfer effects. They apply the two-dimensional version of the CFD code Fluent for predicting the external air flow around the cooling tower and the backflow in different weather conditions.

Many mechanical draught-cooling tower designs are now in the market and all of them use conventional energy to activate the fans and produce airflow. The prototype described in this paper works in the same fashion. However, it uses renewable energy—such as solar or wind energy—to achieve the same objective. According to Kyoto's protocol for developing and increasing the use of new and renewable forms of energy, the extended cooling tower studied in this paper, called Hydrosolar Roof, represents a clear alternative for industrial air-conditioning and other industrial heat dissipation devices.

2. Description of the experimental prototype

The Hydrosolar Roof consists of a metallic structure and a hydraulic circuit mounted on the roof of a building, mainly designed to dissipate energy from it. It is based on the combination of reflective and absorbent flat plates to form inclined channels that act during the summer as solar chimneys producing a natural convection through them. A general view is presented in Fig. 1. The naturally induced airflow is irrigated with water sprays, which generate a reduced version of a cooling tower. Sprayed water is cooled by direct contact with a reduced amount of vaporisation (evaporative cooling) and recovered at the bottom at lower temperature.

The prototype studied in this paper is the improved development of a preliminary model built with parabolic plates. It acted during the summer in the same way, but the design was intended to concentrate and capture the solar radiation for heating during winter time. A study of its behaviour was performed by Sánchez and Viedma [11].

The new prototype, based on the earlier Hydrosolar Roof design, was generated to dissipate a bigger amount of energy when working as water-cooled condenser and also to heat water in winter. However, only the cooling capacities will be commented throughout this paper. During the sunny days of summer the absorbent plates of the system capture the solar radiation. As a consequence of that, both plates forming the channel are hotter than ambient temperature and a vertical air flow is produced by natural convection through it. Hence the system acts as a reduced and two-dimensional solar chimney. Below the channel a water flow is sprayed crosscurrent. A little part of the water is evaporated and the rest is cooled by adiabatic evaporation.

This new prototype was installed to be tested on a laboratory roof at the Universidad Politécnica de Cartagena (37°40′ N), Spain. The total volume occupied by the prototype was roughly $6 \times 6 \times 1.2\,m^3$ in size. During summer 2000 the system was monitored to obtain performance data in a real installation and under real conditions.

Two different zones where main physical processes take place can be identified: radiation and convection zone and evaporative cooling zone, Fig. 1. In order to characterize the Hydrosolar Roof performance, it was necessary to quantify the phenomena developed in each zone. These phenomena implied, on the one hand, heat transfer and air mass flow created by natural convection as well as wind suction effect in the channel, and on the other hand, cooling evaporative effect produced by the

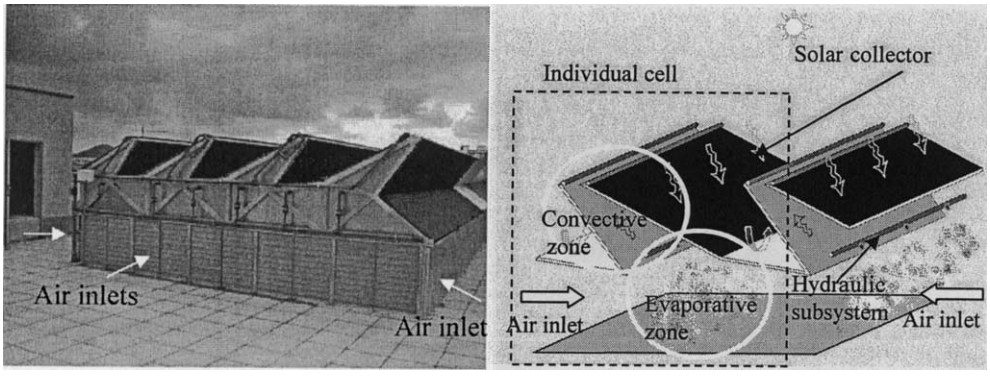

Fig. 1. Full scale Hydrosolar Roof prototype and system scheme, showing the zones where physical processes take place.

energy and mass exchange between air and water in the spray zone. To obtain the heat transfer coefficient between plates and air mass flow, it was necessary to measure air conditions at the channel inlet and outlet sections. The cooling evaporative power was determined by the water mass flow rate and its temperature reduction between the sprinklers and the point where the water was drained from the roof. A detailed description of the experimental set up and results on this prototype was presented by Lucas et al. [12].

Mechanical draught-cooling towers have been widely studied. Different analytical and numerical models of these heat-and-mass transfer processes have been developed by several authors so as to test and improve their performance. The extended cooling tower presented here is based on the same physical processes of cooling evaporation. However, the natural convective airflow generated, the different scale in which physical processes take place with respect to convectional cooling towers, the absence of fans and the influence of new ambient conditions configure a different physical problem. New models of heat-and-mass transfer have to be developed to analyse this reduced scale of cooling tower.

During the last decade, this new concept for energy dissipation system has been implemented in some official buildings in the South of Spain. As it has been shown, various global analyses have been developed on the system. These studies comprise calculations of output energy and system efficiency, as well as parametric analyses and analytic models. The results presented under these references show that this device can be considered as a technically and economically viable form of renewable energy usage.

However, detailed experimental measurements of flow distribution in this extended cooling tower are not available for model validation due to the complexity of internal flow measurements. For this reason, important information has still to be gathered, such as the effect of ambient conditions on the evaporation processes, the influence of the pulverized water-drop size and the pulverized water mass flow. All these details are needed for the proper design of a working system.

Numerical modelling validated by experiments has become a popular tool in cooling tower research and development. Following this trend, this paper shows a numerical study and the experimental validation of the evaporative processes that take place in this extended cooling tower. A mathematical model of these processes is presented here, which allows for the calculation of the two-dimensional internal aerodynamics. This analysis does contemplate the influence of ambient conditions, such as wet bulb temperature, and the effect of other parameters, such as drop size and mass flow of the pulverised water. Localised analysis leads to obtain information about localised phenomena which may appear in certain regions. This way, even the smallest details can be considered, allowing the achievement of the most adequate design and execution.

3. Governing equations and boundary conditions

Processes related to fluid flux and heat-and-mass transfer between different phases are governed by mass, momentum, energy and species conservation principles. These principles may be expressed by means of differential equations. In order to analyse the mathematical model of the problem that has been treated here, three groups of equations may be considered [13]: the set of equations that governs the continuous phase (air mass flow in the chimney produced by natural convection), the set of equations of the discrete phase (droplets of water sprayed), and the set of equations that provides the chemical species (dry air and water vapor). The continuous and discrete phase equations are coupled by the source terms of the conservation equations [14].

3.1. Continuous phase model

The equations of this phase are presented below.

$$\frac{\partial}{\partial x_i}(\rho v_i) = S_{i'}, \tag{1}$$

$$\rho v_j \frac{\partial v_i}{\partial x_j} = \frac{\partial}{\partial x_j}\left[\mu\left(\frac{\partial v_i}{\partial x_j} + \frac{\partial v_j}{\partial x_i}\right) - \frac{2}{3}\mu\left(\frac{\partial v_j}{\partial x_j}\right)\delta_{ij}\right] + \rho g_i - \frac{\partial p}{\partial x_i} + F_{i'}, \tag{2}$$

$$\rho v_i \frac{\partial e}{\partial x_i} = -p\frac{\partial v_i}{\partial x_i} + \Phi_{\mathrm{v}} + \frac{\partial}{\partial x_i}\left(k\frac{\partial T}{\partial x_i}\right) + \frac{\partial}{\partial x_i}\left(\sum_{i'=1}^{n} h_{i'} J_{i'}\right) + S_{\mathrm{h}}, \tag{3}$$

$$\rho v_i \frac{\partial m_{i'}}{\partial x_i} = -\frac{\partial J_{i'},_i}{\partial x_i} + S_{i'}, \tag{4}$$

$$J_{i'},_i = -\rho D_{i',\mathrm{m}} \frac{\partial m_{i'}}{\partial x_i}, \tag{5}$$

where $S_{i'}$, F_i and S_{h} represent the source terms and $J_{i'},_i$, the diffusion flux of species i'. Flow produced bellow the framework may be considered as steady and laminar (zone showed in Fig. 2b). But, over the framework, the wind induces a turbulent flow. For this reason, the model adopted assumes steady state laminar flow in the lower part, bellow the framework, and turbulent flow in the upper part, over the framework. In the turbulent zone, the well-known k–ε model has been employed. Among all two-equation turbulence models, this one has been chosen due to its less computational effort.

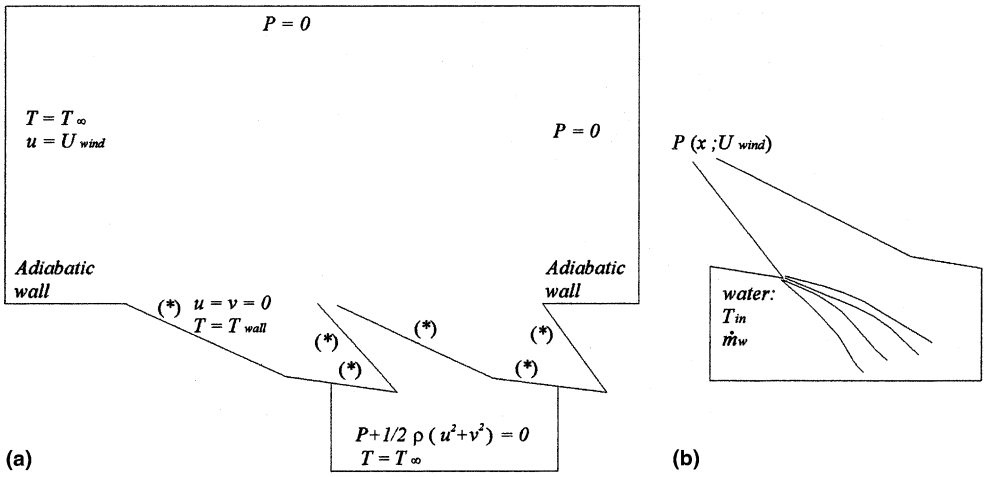

Fig. 2. Description of the boundary conditions used in the numerical model. (a) Extended domain where wind effect has been simulated. (b) Reduced domain where the defect of pressure produced by the wind has been substituted by a local distribution of pressure at the exit of the channel.

3.2. Dispersed phase model

The dispersed phase consists of spherical water droplets of D_p diameter dispersed in the continuous phase. The trajectory of a discrete phase particle (droplet) may be predicted by integrating the force balance on the particle, which is written in a Lagrangian reference frame. This force balance equates the particle inertia with the forces acting on the particle [15], and can be written as Eq. (6). The energy balance in the particle is considered in Eq. (8).

$$\frac{dV_p}{dt} = \frac{18\mu}{\rho_p D_p^2}\frac{C_D Re}{24}(V - V_p) + g\frac{\rho_p - \rho}{\rho_p} + \frac{\rho}{\rho_p}V_p\frac{\partial V}{\partial r_p}, \tag{6}$$

$$\frac{dr_p}{dt} = V_p, \tag{7}$$

$$m_p c_p \frac{dT_p}{dt} = hA_p(T - T_p) + \frac{dm_p}{dt}h_f, \tag{8}$$

$$Re = \frac{\rho D_p \mid V_p - V \mid}{\mu}, \tag{9}$$

$$C_D = a_1 + \frac{a_2}{Re} + \frac{a_3}{Re^2}, \tag{10}$$

$$F_D = \frac{18\mu}{\rho_p D_p^2}\frac{C_D Re}{24}, \tag{11}$$

where coefficients a_1, a_2 and a_3 are constants used for smooth spherical particles over several ranges of Re given by Morsi and Alexander [16], $F_D(V - V_p)$ is the drag force per unit particle mass, $g(\rho_p - \rho)/\rho_p$ is the gravity force per unit particle mass, $(\rho/\rho_p)V_p(\partial V/\partial r_p)$ is the force caused by the pressure gradient in the fluid, and dm_p/dt, the evaporation rate on the particle.

3.3. Coupling between dispersed and continuous phases

The process of coupling between the discrete and the continuous phase is solved by an iterative method. As the trajectory of a particle is computed, the algorithm keeps track of the heat, mass, and momentum gained or lost by the particle stream that follows that trajectory and these values can be incorporated in the subsequent continuous phase calculations. Thus, while the continuous phase always affects the discrete phase, the effect of the discrete phase trajectories on the continuum can be also incorporated. This two-way coupling is accomplished by alternately solving the discrete and continuous phase equations until the solutions in both phases have ceased to change. The source term in the continuity conservation equation (1) may be written as

$$S_{i'} = \frac{\Delta m_p \dot{m}_{p_0}}{m_{p_0} d\forall}, \tag{12}$$

where Δm_p is the particle mass change in each volume differential $d\forall$ in a dt; $\dot{m}_{p_0}$, the initial mass flow rate of the injected particle tracked and m_{p_0}, the initial mass of the particle. This particle mass change in each $d\forall$ may be expressed by

$$\Delta m_p(d\forall) = m_p(t) - m_p(t - dt) = N_v M_v A_p\, dt, \tag{13}$$

where $dt = ds/|V_p + V|$ and ds is the fraction of trajectory inside each volume differential $d\forall$ considered; M_v is the molecular weight of vapor, A_p is the droplet area and N_v is the molar flux of vapor:

$$N_v = K_c(C_{v,s} - C_v), \tag{14}$$

where $C_{v,s}$ is the vapor concentration on the droplet surface and C_v, the vapor concentration in the bulk gas:

$$C_{v,s} = \frac{p_{vs}(T_p)}{R(T_p)} \quad C_v = \frac{px_v}{RT}, \tag{15}$$

with x_v being the mass fraction of vapor. Mass transfer coefficient K_c is obtained by a correlation of the Nusselt number given by Ranz and Marshall [17,18]

$$K_c = \frac{NuD_{v,m}}{D_p} = \frac{(2 + 0.6Re^{1/2}Sc^{1/3})D_{v,m}}{D_p}. \tag{16}$$

Source terms of momentum equation (2) F and energy equation (3) S_h, are given by the following expressions:

$$F = \left(\frac{18\mu}{\rho_p D_p^2}\frac{C_D Re}{24}(V - V_p) + g\frac{(\rho_p - \rho)}{\rho_p} + \frac{\rho}{\rho_p}V_p\frac{\partial V}{\partial r_p}\right)\frac{\dot{m}_{p_0}\,dt}{d\forall}, \tag{17}$$

$$S_h = \left[\frac{\bar{m}_p}{m_{p_0}}C_p\Delta T_p + \frac{\Delta m_p}{m_{p_0}}\left(-h_f + \int_{T_{ref}}^{T_p} C_{p,i}\,dT\right)\right]\frac{\dot{m}_{p_0}}{d\forall}, \tag{18}$$

where $\bar{m}_p$ is the average mass of the particle in control volume $d\forall$and ΔT_p, the temperature change of the particle in control volume $d\forall$.

3.4. Boundary conditions

The boundary conditions required for the present problem will now be described. Non-slip conditions are imposed on the walls. On heated isothermal walls, T is fixed as T_{wall}. On adiabatic walls, the heat flux from wall to fluid is zero. The wind is considered by a horizontal velocity ($u = U_{wind}$) on the upper left side boundary, where also the incoming flow temperature is set equal to T_∞. For outgoing flow boundaries, pressure is set to $P = p - p_\infty = 0$, where p_∞ is the hydrostatic pressure distribution. The lower inlet's boundary conditions are set for temperature $T = T_\infty$ with streamwise variation equal to zero, and for total pressure equal to zero: $P + \frac{1}{2}\rho(u^2 + v^2) = 0$. In this manner, it is assumed that Bernoulli equation holds in the entrance region. Solar radiation was simulated by means of a temperature difference between channel plates and ambient conditions $\Delta T = T_{wall} - T_\infty$.

Properties of moist air, such as moisture fraction, specific humidity, enthalpy, and others, are calculated through equations for psychometric properties, derived from the fundamental equations for ideal gas mixtures.

In order to concentrate our calculation efforts on the evaporation zone and save computational time, the wind effect was substituted by a longitudinal depression $P(x, U_{wind})$ in the channel outlet. The computational domain studied may thus be reduced. Fig. 2 shows boundary conditions used to calculate Hydrosolar Roof performance and both computational domains studied.

3.5. Model of wind effect

As noted in the previous paragraph, the wind blowing over the solar chimney produces a suction effect at its exit. As a result, the higher the wind velocity, the higher the air mass flow generated within the sloped channel. This suction effect may be substituted by a local pressure distribution at the exit of the sloped channel. Taking this fact into account, the extended domain (Fig. 2a) may be replaced by a more reduced one (Fig. 2b), that includes that local pressure distribution at the exit of the channel. This way, computational time may be gained. For example, supposing there is a temperature gap between channel plates and ambient conditions of $\Delta T_{wall} = 20\,°C$ and a wind velocity of $U_{wind} = 1\,m/s$, the pressure distribution at the exit of the channel takes the form of Fig. 3 and the air mass flow generated within the channel is $\dot{m}_a = 0.0289\,kg/s$. If this pressure distribution is imposed at the exit of the channel in the domain of Fig. 2b, the air mass flow obtained is $\dot{m}_a = 0.0281\,kg/s$. In all cases studied, the discrepancies obtained were lower than 3%. Taking these results into account, the effect of the wind may be substituted by a localised pressure at the exit of the sloped channel and the domain of Fig. 2a may be replaced by the domain of Fig. 2b.

3.6. Model of water pulverization

This paper has studied heat-and-mass transfer processes within the Hydrosolar Roof, where just water droplets' flow has been considered, neither jet nor film flows. As pointed out by Fisenko et al. [4], while

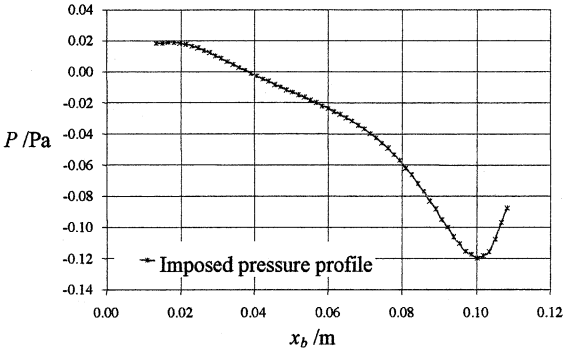

Fig. 3. Imposed pressure profile at the exit of the channel in the domain (b) of Fig. 2 for a temperature gap of 20 °C between the ambient and the channel plates and a wind velocity of 1 m/s.

determining the mathematical model of the evaporative cooling of droplets, knowing their size distribution is important. In real systems, droplets are formed by water spraying nozzles. Droplet radius depends on water flow rate and water temperature: the larger the water flow rate, the higher the pressure drop in the nozzles and the smaller the size of droplets. Water temperature affects surface tension, which determines the character of water spraying. The dependence of droplet radius on hydraulic loading is determined by design feature of the spraying nozzle.

To model this distribution in all cases studied here Rosin–Rammler's equation has been applied, basing on the assumption that an exponential relationship exists between droplet diameter D_p, and mass fraction M_{D_p} of droplets with diameter greater than D_p:

$$M_{D_p} = \exp\left(-\left(\frac{D_p}{\overline{D}}\right)^n\right), \tag{19}$$

where $\overline{D}$ is the average droplet diameter and n is a fit coefficient. The typical parameters of the distribution have been determined taking into account available information on the commercial spraying nozzles (model X-22 flat-cone) employed in the experimental tests. The distribution adopted in the numerical model is presented in Fig. 4.

This distribution assumes that droplets have a spherical shape. Spray water is composed of 300 trajectories of droplets in a two-dimensional flow. This spray is injected into the upper part of the evaporative zone, in the origin of the Cartesian axis (see Fig. 4). The first trajectory is determined by an angle of $-30°$ and the last one by an angle of $-50°$ both with respect to the x axis, in Cartesian coordinates. Average droplet velocity is approximately 14 m/s.

4. Method of numerical solution

This system of equations has been numerically solved through a 2D model using general-purpose code Fluent, based on a finite volume procedure [13]. The equations are discretized using Presto's scheme, which is similar to the staggered-grid scheme [19], with a second-order upwind scheme for convective terms. The Simple algorithm is used to solve the coupling between continuity and momentum equations through pressure. The convergence criterion in each case was $(\phi^{(i+1)} - \phi^{(i)})/\phi^{(i)} < 10^{-5}$, where i denotes the iteration number and ϕ can stand for any of the dependent variables.

A structured, non-uniform mesh is used. In order to ensure the accuracy of numerical results, a grid dependence study was performed in both domains analysed. An exponential law was used to obtain a fine grid near walls, inlet and outlet of the domain, as shown in Fig. 5. Several meshes of different size have been used and the mesh of size 24,208 cells for the domain of Fig. 2a and 19,742 cells for the domain of Fig. 2b are found to give grid independent results. Refining the mesh further did not produce any appreciable change in results.

5. Results and discussion

In a cooling tower, heat-and-mass transfer processes depend on the specific mass flow rates of water $\dot{m}_w$ and air $\dot{m}_a$, temperature T_∞ and relative humidity ψ of the air entering into the cooling tower, temperature T_{in} of the water entering into the domain considered, wind velocity and atmospheric pressure [20]. The influence of most of these parameters has been taken into account in this study. In what follows, an experimental

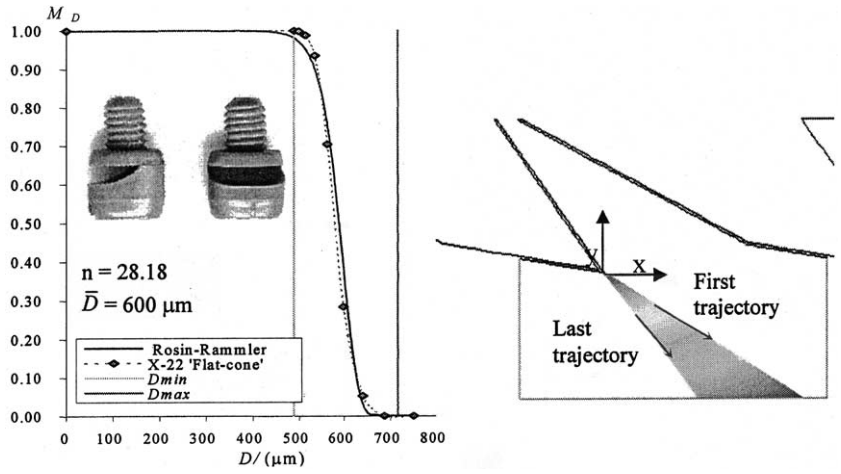

Fig. 4. Experimental diameter distribution of droplets of the spraying nozzle model X-22 flat-cone and diameter distribution of droplets assumed in this study, following the Rosin–Rammler's function. Scheme of the trajectories of droplets.

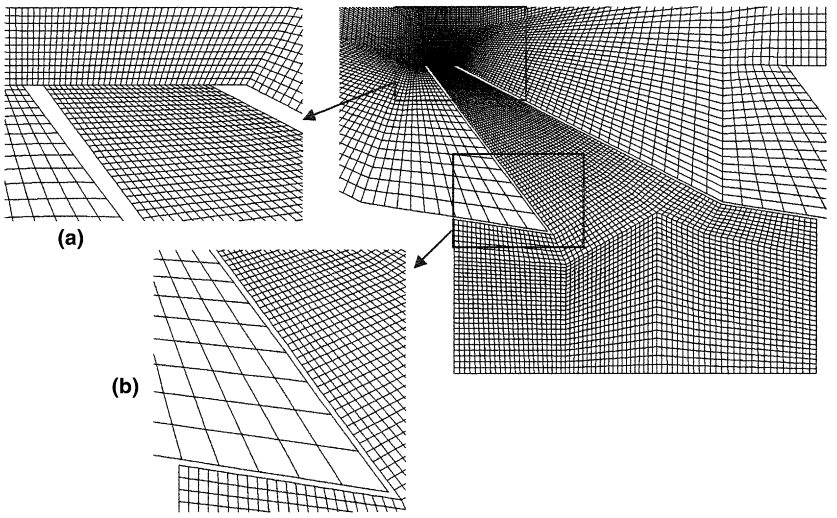

Fig. 5. Mesh of the extended domain (Fig. 2a). (a) Detail of the mesh at the exit of the channel. (b) Detail showing the difference in the mesh density between outside the channel (turbulent flow where wall functions have been used) and inside the channel (laminar flow).

validation of the predicted data, a general description of field flow and the influence of meaningful parameters on evaporation processes will be presented.

5.1. Validation of predicted results by experimental data

Field test data measured in the Hydrosolar Roof prototype have been used to validate the present numerical simulation. The experimental methodology employed in these tests, the results obtained and the experimental correlations deduced from this analysis were presented in [12]. Some of these experimental results have been selected for comparison and validation of our numerical analysis.

During tests, measurements were taken of wind velocity (U_{wind}), temperature of channel plates (T_{wall}), dry (T) and wet bulb temperature (T_{wb}), air mass flow within the channel ($\dot{m}_a$), water mass flow ($\dot{m}_a$), and its temperatures at inlet (T_{in}) and outlet (T_{out}). Some sets of measured and predicted outlet temperatures are shown in Table 1.

In the case of a monodisperse distribution of droplets, average water temperature coincides with final temperature of droplets. However, when the size distribution of droplets and nonuniformity of airflow in the evaporation processes are taken into account, an average temperature should be obtained. For the predicted cases included in Table 1, average values of droplet temperature for each case have been presented.

It can be seen from Table 1 that the difference between measured outlet water temperatures and our predictions, $T_{out\text{-}pr} - T_{out\text{-}me}$, varies between 1.4 °C and approximately 0 °C. The average absolute difference is 0.35 °C. The relative discrepancy, $(T_{out\text{-}pr} - T_{out\text{-}me})/T_{out\text{-}me}$, varies between 4.12% and −0.56%. Considering the uncertainty of the experimental data and the approximation of the present simulation, the agreement between numerical predictions and experimental values is

Table 1
Comparison between predicted and measured outlet water temperature, considering an average diameter of droplets of 600 μm and different wet bulb and water inlet temperatures

No.	u_w (m/s)	ΔT_{wall} (°C)	$\overline{D}$ (μm)	T_{wb} (°C)	T_{in} (°C)	$\dot{m}_w/\dot{m}_a$	$T_{out\text{-}pr}$ (°C) (predicted)	$T_{out\text{-}me}$ (°C) (measured)	Discrepancy (%)
1	1	20	600	25.6	45	0.89	35.123	33.732	4.12
2	1	20	600	25.6	40	0.89	32.933	32.572	1.11
3	1	20	600	25.6	35	0.89	30.591	30.761	−0.55
4	1	20	600	25.6	35	0.54	30.540	30.490	0.17
5	1	20	600	25.6	35	1.28	30.623	30.797	−0.56
6	1	20	600	20.6	30	0.89	26.282	26.284	−0.01
7	1	20	600	15.6	25	0.89	22.145	21.836	1.42

considered good. This shows that the present numerical model reproduces the physical cooling processes inside the Hydrosolar Roof and, as such, the presently developed numerical scheme and computer code can be used as a design tool.

5.2. Flow field simulation

Figs. 6–11 show some aspects of the numerical simulation of case number 6 (see Table 1). Fig. 6 represents the wind velocity field in the domain of Fig. 2a. As pointed out above, this flow field induces a pressure distribution at the exit of the sloped channel causing an increase in the air mass flow generated within this channel.

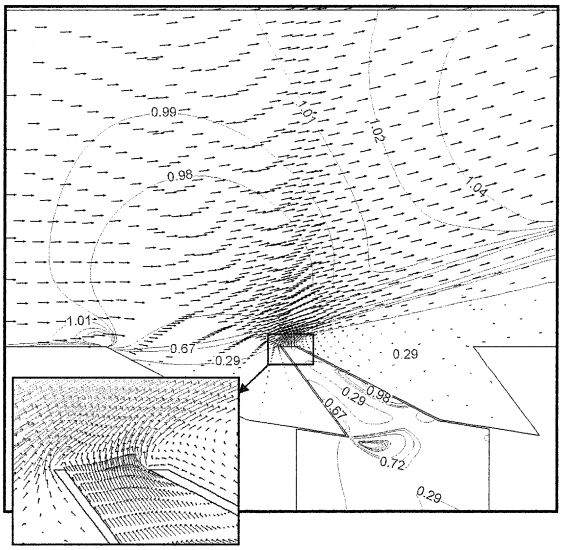

Fig. 6. Wind velocity distribution over the Hydrosolar Roof in m/s. Detail of air velocity distribution at the exit of the channel.

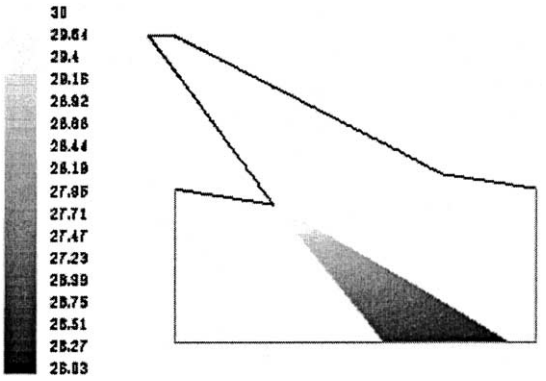

Fig. 7. Water temperature decrease in the reduced domain (Fig. 2b) in °C.

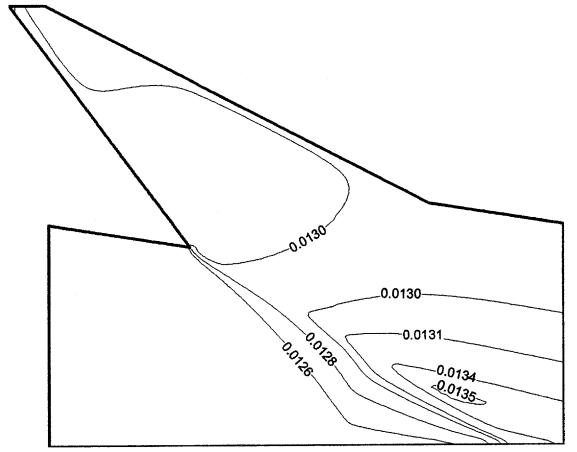

Fig. 8. Mass fraction of water vapor in air in the reduced domain (Fig. 2b).

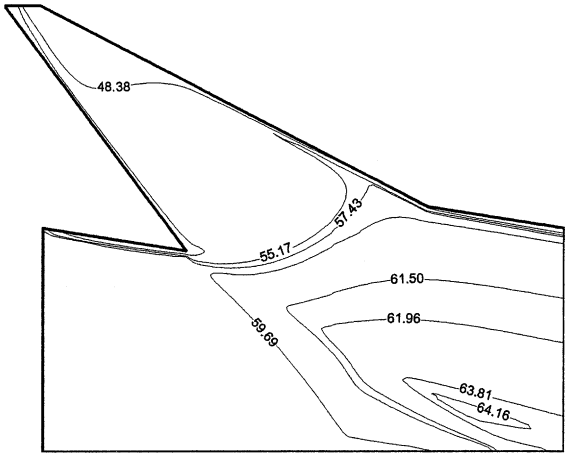

Fig. 9. Relative humidity in the reduced domain (Fig. 2b), %.

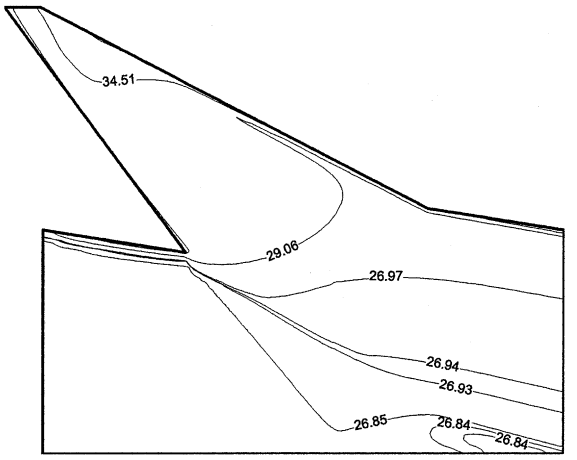

Fig. 10. Air temperature distribution in the reduced domain (Fig. 2b) in °C.

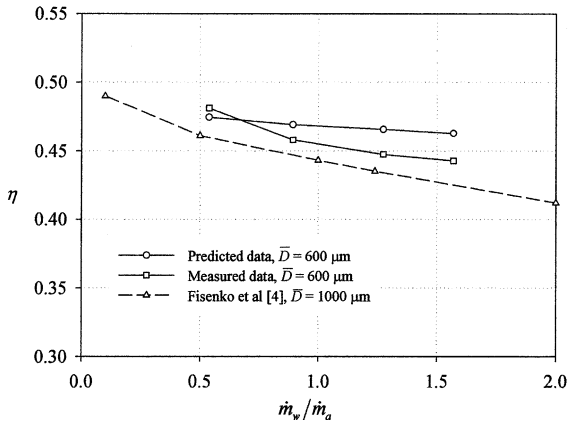

Fig. 11. Influence of water to air mass flow ratio on efficiency, for an average droplet diameter of 600 μm, wet bulb temperature of 25.6 °C and maximum water temperature difference of 9.4 °C: predicted and measured results as well as the results proposed by Fisenko et al. [4].

In mechanical draught counter-flow cooling towers, as droplets fall down, water evaporates and convective heat transfer with colder air occurs. The increase in droplet velocity reduces the time of interaction with fresh air. On the other hand, as air ascends it is heated and saturated with water vapor. This reduces the intensity of heat-and-mass transfer of droplets during evaporative cooling [4]. However, in the system studied, the process is quite different. It happens as in a cross-flow cooling tower. The air mass flow—generated in the chimney by buoyancy forces and by the effect of the wind—crosses the pulverised water mass flow and carries away the water vapor produced in the evaporation processes.

It is clearly proven that water temperature decreases continuously as it approaches the bottom of the tower (see Fig. 7). Air acting as a coolant enters from the sides of the tower, initially at its dry bulb temperature, and increases in temperature before leaving from the top and sides of the evaporative zone. However, localised cooling of air and water is produced at the bottom of the tower, due to the evaporation process (see Fig. 10). It can be appreciated that evaporation rates in this region are generally high (Figs. 8 and 9). When water evaporates, it needs heat that is taken from both water and air. Accordingly, it could be expected the possibility of cooling both air and water in the tower (see Figs. 7 and 10).

In the Hydrosolar Roof, as opposed to most conventional cooling towers, the humid air at the exit of the cooling evaporation zone is not saturated due to the reduced height of droplet fall (see Fig. 9). As pointed out by Fisenko et al. [4], the effect of saturation arising with the increase in ratio between height of droplets fall and diameter of droplets ($H/\overline{D}$) is well seen. In our case, this ratio varies between 700 and 2700 approximately. A comparative study of conventional cooling towers and the Hydrosolar Roof is presented by Sánchez et al. [21]. Considering that saturation of humid air in the evaporation zone is not reached, higher water mass flow to air mass flow ratios could be used, thus increasing the power dissipated by cooling evaporation. In further designs these considerations will be taken into account.

Water temperature variation inside the Hydrosolar Roof is presented in Fig. 7. Average water temperature decreases from inlet water temperature at 30 °C to about 26.03 °C on the roof floor. Because of the evaporation loss, the water mass flux decreases as it goes down. Numerical results show that the total evaporation loss is about 0.65% of inlet water flow rate.

5.3. Predicted distributions of the dependent variables

According to Merkel's model [1], water temperature decrease depends mainly on incoming air wet bulb temperature, T_{wb}. Therefore, the physical limit to outlet water temperature is the wet bulb ambient temperature. Hence, system efficiency can be defined as [22]

$$\eta = \frac{T_{in} - T_{out}}{T_{in} - T_{wb}} = \frac{\Delta T}{\Delta T_{max}}. \quad (20)$$

Our numerical study focused on obtaining the influence on efficiency of some thermodynamic parameters, such as maximum water temperature difference (ΔT_{max}, temperature difference between water inlet temperature and wet bulb temperature), water to air mass flow ratio ($\dot{m}_w/\dot{m}_a$), wet bulb temperature (T_{wb}) and average water drop size ($\overline{D}$). For each water mass flow considered, a different water to air mass flow ratio was obtained ($\dot{m}_w/\dot{m}_a$). The characteristic working zone ratio for a mechanical draught-cooling tower has been described by Mohiuddin and Kant [3]. The next few paragraphs deal with the influence of these dependent variables on the efficiency of the system, for a wind velocity of 1 m/s and a temperature gap of 20 °C between the plates of the channel and ambient temperature.

5.3.1. Influence of maximum water temperature difference (ΔT_{max})

As it could be expected, when the maximum water temperature increases, the efficiency of the system increases too. Although numerical and experimental results show a similar upward trend, certain discrepancies could be appreciated between both sets of results (see Table 2).

5.3.2. Influence of water mass flow to air mass flow ratio ($\dot{m}_w/\dot{m}_a$)

The effect of the water to air mass flow ratio, $\dot{m}_w/\dot{m}_a$, was investigated by varying the mass flow rate of water

Table 2
Influence on efficiency of maximum water temperature difference ΔT_{max}, for an average diameter of droplets of 600 μm, wet bulb temperature of 25.6 °C and water and air mass flow ratio of 0.89, showing predicted and measured results

No.	$\overline{D}$ (μm)	T_{in} (°C)	T_{wb} (°C)	ΔT_{max} (°C)	$(\dot{m}_w/\dot{m}_a)$	$T_{out\text{-}pr}$ (°C) (predicted)	$T_{out\text{-}me}$ (°C) (measured)	η_{pr} (predicted efficiency)	η_{me} (measured efficiency)
1	600	45	25.6	19.4	0.89	35.123	33.732	0.509	0.581
2	600	40	25.6	14.4	0.89	32.933	32.572	0.491	0.516
3	600	35	25.6	9.4	0.89	30.591	30.761	0.469	0.451

$\dot{m}_w$ while keeping the airflow rate $\dot{m}_a$ approximately constant. As expected, the results reveal that after an increase in water mass flow rate, the surface area required both for convection and evaporation will be reduced, resulting in higher water outlet temperature and reduced heat transfer rates. This fact may be appreciated in Fig. 11. This is a typical behaviour of cooling towers [4,20]. As will be commented in point 4.3.4, the higher the droplet diameter, the lower the efficiency. Numerical results are in accordance with experimental results (see Table 3). Less than 2% variation has been obtained in every case.

5.3.3. Influence of wet bulb temperature (T_{wb})

Fig. 12 depicts the effect of wet bulb air temperature on efficiency. An increase in wet bulb temperature, keeping the difference constant between inlet water temperature and this wet bulb temperature ($T_{in} - T_{wb}$) increases both partial pressure difference ($p_{vs} - p_v$) and potential enthalpy ($h_s - h$) between interface and air, resulting in increased efficiency. This increase is roughly linear in the range studied. A variation of about 16.5% in the predicted values and about 11.5% in the measured values for temperatures between 15.6 °C and 25.6 °C has been obtained (see Table 4). Similar conclusions have been also pointed out by Facão and Oliveira [23] for a closed wet cooling tower.

5.3.4. Influence of average water drop size ($\overline{D}$)

As reported by Fisenko et al. [4], the dependence of droplet radius on efficiency is rather strong. Fig. 13 compares the results obtained for the Hydrosolar Roof and those proposed in [4] for a conventional mechanical draught-cooling tower. Both results show a similar

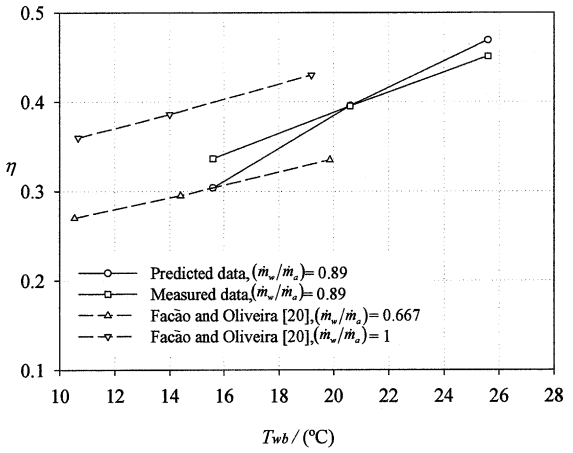

Fig. 12. Influence of wet bulb temperature on efficiency, for an average diameter of droplets of 600 μm, water to air mass flow ratio of 0.89 and maximum water temperature difference of 9.4 °C: predicted and measured results as well as the results proposed by Facão and Oliveira [20].

trend. However, certain discrepancies may be appreciated. As can be observed in the results from the Hydrosolar Roof (see Table 5), for a fixed water mass flow, the smaller the drop size, the higher the efficiency, due to the increase in heat-and-mass transfer surface between water and air. Following the trend described in point 4.3.1, Fig. 13 shows that the higher the temperature gap between inlet water temperature and wet bulb temperature, the higher the efficiency, for different average water drop sizes. This effect could be considered less important than the effect of droplet average diameter.

Table 3
Influence of water and air mass flow ratio on outlet water temperature, for an average diameter of droplets of 600 μm, wet bulb temperature of 25.6 °C and maximum water temperature difference of 9.4 °C, showing predicted and measured results

No.	$\overline{D}$ (μm)	T_{in} (°C)	T_{wb} (°C)	ΔT_{max} (°C)	m_w/m_a	$T_{out\text{-}pr}$ (°C) (predicted)	$T_{out\text{-}me}$ (°C) (measured)	η_{pr} (predicted efficiency)	η_{me} (measured efficiency)
1	600	35	25.6	9.4	0.54	30.540	30.490	0.475	0.481
2	600	35	25.6	9.4	0.89	30.591	30.702	0.469	0.458
3	600	35	25.6	9.4	1.27	30.623	30.797	0.466	0.447
4	600	35	25.6	9.4	1.57	30.651	30.839	0.463	0.443

Table 4
Influence of wet bulb temperature on outlet water temperature, for an average diameter of droplets of 600 μm, water and air mass flow ratio of 0.89 and maximum water temperature difference of 9.4 °C, presenting predicted and measured results

No.	$\overline{D}$ (μm)	T_{in} (°C)	T_{wb} (°C)	ΔT_{max} (°C)	m_w/m_a	$T_{out\text{-}pr}$ (°C) (predicted)	$T_{out\text{-}me}$ (°C) (measured)	η_{pr} (predicted efficiency)	η_{me} (measured efficiency)
1	600	25	15.6	9.4	0.89	22.1446	21.835	0.304	0.337
2	600	30	20.6	9.4	0.89	26.2818	26.284	0.396	0.396
3	600	35	25.6	9.4	0.89	30.5908	30.761	0.469	0.451

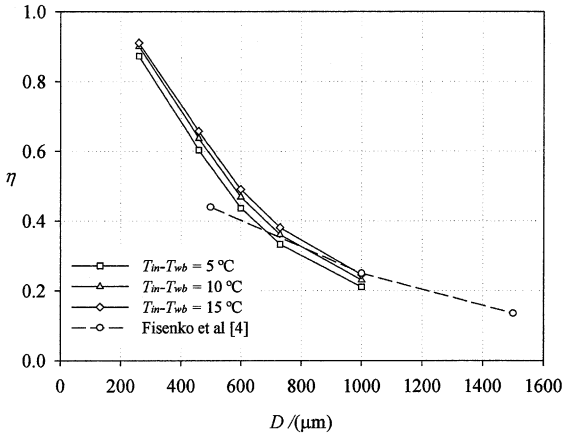

Fig. 13. Influence of average diameter of droplets on efficiency, for a wet bulb temperature of 25.6 °C, a water to air mass flow ratio of 0.89 and different maximum water temperatures: predicted results as well as the results proposed by Fisenko et al. [4].

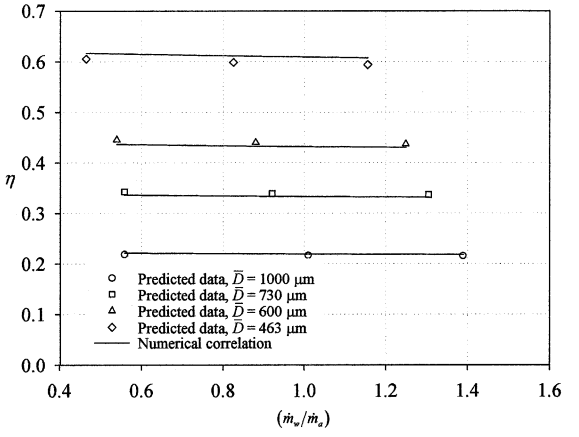

Fig. 14. Numerical correlation of the efficiency as a function of water mass flow and air mass flow ratio and droplet average diameter, for a ΔT_{max} of 9.4 °C and a T_{wb} of 25.4 °C.

5.3.5. Numerical correlation

Once the influence on efficiency of significant parameters of the evaporative cooling processes has been determined within the Hydrosolar Roof, a nondimensional numerical correlation has been calculated (see Fig. 14). The influence of four nondimensional parameters has been considered: ratio between droplet fall height and droplet average diameter, water mass flow to air mass flow ratio, temperature gap between

Table 5
Influence of average diameter of droplets on outlet water temperature, for a wet bulb temperature of 25.6 °C, a water and air mass flow ratio of 0.89 and different maximum water temperatures

No.	$\overline{D}$ (μm)	T_{in} (°C)	T_{wb} (°C)	ΔT_{max} (°C)	m_w/m_a	$T_{out\text{-}pr}$ (°C)	η_{pr}
1	260	30	25.6	4.4	0.89	26.160	0.873
2	460	30	25.6	4.4	0.89	27.347	0.603
3	600	30	25.6	4.4	0.89	28.078	0.437
4	730	30	25.6	4.4	0.89	28.535	0.333
5	1000	30	25.6	4.4	0.89	29.072	0.211
6	260	35	25.6	9.4	0.89	26.537	0.900
7	460	35	25.6	9.4	0.89	29.016	0.637
8	600	35	25.6	9.4	0.89	30.596	0.469
9	730	35	25.6	9.4	0.89	31.609	0.361
10	1000	35	25.6	9.4	0.89	32.831	0.231
11	260	40	25.6	14.4	0.89	26.895	0.910
12	460	40	25.6	14.4	0.89	30.538	0.657
13	600	40	25.6	14.4	0.89	32.938	0.490
14	730	40	25.6	14.4	0.89	34.517	0.381
15	1000	40	25.6	14.4	0.89	36.460	0.246

water inlet temperature and wet bulb temperature divided by ambient temperature, and wet bulb temperature divided by ambient temperature. Discrepancies lower than 5% have been obtained between the proposed correlation and the calculated numerical data.

$$\eta = 4.645 \times 10^{-5} \left(\frac{H}{\overline{D}}\right)^{1.325} \left(\frac{\dot{m}_w}{\dot{m}_a}\right)^{0.0174} \left(\frac{T_{in} - T_{wb}}{T_\infty}\right)^{0.1777} \times \left(\frac{T_{wb}}{T_\infty}\right)^{0.6652} \quad (21)$$

6. Conclusions

This paper analyses the heat-and-mass transfer processes that take place in a new system for heat dissipation. The mathematical model presented, consisting of two coupled sets of conservation equations for the continuous and discrete phases, respectively, has been incorporated in the general purpose CFD code Fluent. Thus, a numerical finite-volume technique has been employed to simulate direct contact evaporative cooling in the second generation Hydrosolar Roof: a natural draught evaporation system tested in ambient conditions. Experimental results from the Hydrosolar Roof have been employed to validate the numerical results. Variations in representative parameters between measured (experimental) and predicted (numerical) results lower than 5% were obtained. This comparison assesses the validity of the model proposed.

The main results of this study show the strong influence of the average water drop size on efficiency and reveal the effect of other variables like wet bulb temperature, water mass flow to air mass flow ratio and temperature gap between water inlet temperature and wet bulb temperature. Nondimensional numerical correlation of efficiency as a function of these significant parameters has been calculated in order to characterise the Hydrosolar Roofs performance under different working conditions.

The flow field numerical solution indicates that humid air saturation in the evaporation zone is not reached and, as a result, higher water mass flow to air mass flow ratios could be employed. The model developed is self-consistent and physically plausible and it can be used for performance evaluation, as well as for design optimisation studies.

Although the Hydrosolar Roof shows important differences with conventional mechanical cooling towers (such as air mass flow induced by sun radiation instead of by fans, or a different physical geometry with a smaller droplet fall), it has been detected a similar influence of the representative parameters in the evaporative cooling processes between both systems.

Acknowledgments

The authors wish to acknowledge the collaboration of José María Galán (manager at Energy, Comfort and Environment S.L.) who suggested and patented in 1986 the original idea (ref. ES 2 002 921), as well as the support provided by the JOR3-CT98-7038 European Commission contract.

References

[1] F. Merkel, Verdunstungskühlung, VDI Forchungsarbeiten, Berlin, No. 275, 1925.
[2] H.B. Nottage, Merkel's cooling diagram as a performance correlation for air water evaporative cooling system, ASHVE Trans. 47 (1941).
[3] A.K.M. Mohiuddin, K. Kant, Knowledge base for the systematic design of wet cooling towers, Int. J. Refrigeration 19 (1) (1996) 43–51.
[4] S.P. Fisenko, A.A. Brin, A.I. Petruchik, Evaporative cooling of water in a mechanical draught-cooling tower, Int. J. Heat Mass Transfer 47 (1) (2004) 165–177.
[5] D.J. Benton, W.R. Waldrop, Computer simulation of transport phenomena in evaporative cooling towers, ASME J. Eng. Gas Turbines Power (110) (1988) 190–196.
[6] G.V.S. Sesha Girish, A. Mani, Numerical simulation of forced convective evaporation system for tannery effluent, Int. J. Heat Mass Transfer 47 (6–7) (2004) 1335–1346.
[7] G. Gan, S.B. Riffat, A numerical study of solar chimney for natural ventilation of buildings with heat recovery, Appl. Thermal Eng. 18 (12) (1998) 1171–1187.
[8] S.A. Kalogirou, Design of a new spray-type seawater evaporator, Desalination 139 (1–3) (2001) 345–352.
[9] A.A. Badran, Performance of cool towers under various climates in Jordan, Energy Bldgs. 35 (10) (2003) 1031–1035.
[10] N. Milosavljevic, P. Heikkila, A comprehensive approach to cooling tower design, Appl. Thermal Eng. 21 (2001) 899–915.
[11] A. Sánchez, A. Viedma, Hydrosolar roof for integrated energy dissipation and capture in buildings, Energy Bldgs. 33 (2001) 673–682.
[12] M. Lucas, P. Martínez, A. Sánchez, A. Viedma, B. Zamora, Improved Hydrosolar Roof for buildings' air conditioning, Energy Bldgs. 35 (9) (2003) 963–970.
[13] FLUENT, User's Guide, Fluent Inc., USA, 1993.
[14] G. Gan, S.B. Riffat, Numerical simulation of closed wet cooling towers for chilled ceiling systems, Appl. Thermal Eng. 19 (12) (1999) 1279–1296.
[15] G. Gan, S.B. Riffat, L. Shao, P. Doherty, Application of CFD to closed-wet cooling towers, Appl. Thermal Eng. 21 (2001) 79–92.
[16] S.A. Morsi, A.J. Alexander, An investigation of particle trajectories in two-phase flow systems, J. Fluid Mech. 55 (2) (1972) 193–208.
[17] W.E. Ranz, W.R. Marshall, Evaporation from drops, Part I, Chem. Eng. Prog. 48 (3) (1952) 141–146.
[18] W.E. Ranz, W.R. Marshall, Evaporation from drops, Part II, Chem. Eng. Prog. 48 (4) (1952) 173–180.

[19] S.V. Patankar, Numerical Heat Transfer and Fluid Flow, Hemisphere, Washington, 1980.
[20] A.I. Petruchik, A.D. Solodukhin, N.N. Stolovich, S.P. Fisenko, Toward the analysis of experimental data on thermal efficiency of evaporative cooling tower, Appl. Energy: Russian J. Fuel Power Heat Syst. 37 (6) (2000) 142–149.
[21] M.M. Sánchez, M. Lucas, P. Martínez, A. Sánchez, A. Viedma, Climatic solar roof: an ecological alternative to heat dissipation in buildings, Solar Energy 73 (6) (2002) 419–432.
[22] L.D. Berman, Evaporative Cooling of Circulating Water, Pergamon, London, 1961, p. 710.
[23] J. Facão, A.C. Oliveira, Thermal behaviour of closed wet cooling towers for use with chilled ceilings, Appl. Thermal Eng. 20 (13) (2000) 1225–1236.